Research Article

Journal of Environmental Nanotechnology

Green Synthesis and Electrochemical Evaluation of TSP–MnO_2 Nanocomposites for Supercapacitor Applications

Ajinkya Prakash Edlabadkar[1], N. Shalom[2], P. Berlin Push[3], Pooja Singh[4], Sumanth Ratna Kandavalli[5], and M. Lakshmi Priya[6*]

[1]Department of Mechanical Engineering, Yeshwantrao Chavan College of Engineering, Wanadongri, Nagpur, MH, India
[2]Department of Mechanical Engineering, Karpagam College of Engineering, Coimbatore, TN, India
[3]Department of Mechanical Engineering, Noorul Islam Centre for Higher Education, Kumaracoil, Kanayakumari, TN, India
[4]Department of Physics, SGT University, Gurugram, HR, India
[5]Department of Mechanical Engineering, Tandon School of Engineering, New York University, Brooklyn, NY, USA
[6]Department of Computer Science and Engineering, Erode Sengunthar Engineering College (Autonomous), Perundurai, Erode, TN, India
*rdeepalakshmi1986@gmail.com

Received: 19.11.2025 Accepted: 28.01.2026 Published: 30.03.2026

ABSTRACT

The need for solutions to store energy is rising due to population growth, industrialization, and technological advancements in a rapidly evolving world. This study examines the viability of TSP (TSP)- manganese dioxide (MnO_2) nanocomposite as a novel material for energy storage application. The nanocomposite was prepared by direct and economical co-precipitation technique. The morphological, compositional and structural characteristics of synthesized TSP- MnO_2 nanocomposite were validated using characterization techniques including scanning electron microscopy, X-ray diffraction, Fourier transform infrared spectroscopy and energy dispersive X-ray analysis. The electrochemical investigations, galvanostatic charge-discharge (GCD) and encompassing cyclic voltammetry (CV) examination demonstrated efficacy of the synthesized material. The CV investigation conducted with 3 M potassium hydroxide electrolyte demonstrated a specific capacitance (C_{sp}) of 515.26 F g^{-1} with a scanning rate of 10 mV s^{-1} and a specific density of 282.26 Wh kg^{-1}. The nanocomposite demonstrated specific capacitance of 9.12 F g^{-1} in the GCD experiment. These changes indicate that the material demonstrates pseudocapacitive properties. Furthermore, the nanocomposite exhibited a minimal internal resistance of 6.0 Ω and ionic conductivity of 1.5×10^{-3} S/cm. The notable improvement in energy density and specific capacitance relative to pure TSP highlights the exceptional potential of the TSP-MnO_2 nanocomposite.

Keywords: TSP; Manganese dioxide; Cyclic voltammetry; Galvanostatic charge-discharge; Specific capacitance.

1. INTRODUCTION

Currently, rapid transformation due to population growth, industrialization, and technological advancements are escalating the global demand for energy. An electrochemical sensor for dexamethasone detection was developed using manganese oxide (MnO_2)/reduced graphene oxide (rGO) nanocomposite on glassy carbon electrodes. The MnO_2/rGO structure exhibited high active surface area and synergistic electrocatalytic effects, enabling a detection limit of 0.005 µM and sensitivity of 4.6153 µA $µM^{-1}$. The sensor achieved 96.34% recovery and 3.58% RSD, proving its reliability for pharmaceutical and clinical applications (Purnama *et al*. 2023). Manganese oxide modified with silico-tungstic acid (STA) was synthesized by co-precipitation. Structural, morphological, and surface analyses (XRD, SEM–EDS, BET) revealed increased surface area (153.6 m^2/g) and mesoporosity for MnO_2–10% STA. Electrochemical studies in 0.5 M K_2SO_4 showed a significant rise in double-layer capacitance (181 F g^{-1}) compared to unmodified MnO_2 (38 F g^{-1}), indicating superior capacitive behavior due to STA modification (Thiam and Savadogo, 2024). MnO_2 composites supported on graphite (G), graphitic carbon nitride (gCN), and gCN/C were developed as non-precious metal catalysts. Characterization confirmed strong Mn–C and Mn–N interactions, enhancing electrocatalytic efficiency. The MnO_2–gCN/C catalyst achieved the most positive ORR onset potential (0.9 V) and lowest OER onset potential (1.53 V), maintaining 85% stability after 24 hours, proving high bifunctional activity for oxygen-related reactions (Zabielaite *et al*. 2024). Manganese (Mn)-doped cobalt ferrite nanoparticles ($Mn_xCo_{1-x}Fe_2O_4$; x = 0.0–0.6) was synthesized by green combustion-assisted method with TSP (TSP) as fuel. Structural and optical studies confirmed nanoflake morphology (5.7–7.6 nm) with reduced bandgap and luminescence upon Mn doping. The nanoparticles exhibited good electrochemical and

photocatalytic performance under visible light (Adarshgowda *et al*. 2024).

MoO_3 nanoparticles were prepared by solution combustion using TSP as novel carbon-yielding fuel. The *in situ* generated carbon enhanced conductivity, eliminating the need for additional conducting agents. The material showed an initial discharge capacity of 1171 mAh g^{-1} and stabilized at 162 mAh g^{-1} after 200 cycles with nearly 100% Coulombic efficiency, demonstrating strong potential as a lithium-ion battery anode (Shahsank *et al*. 2021). Lignin nanoparticles derived from wheat straw were converted into porous carbon (LPC) by $ZnCO_3$ activation and pyrolysis (600–800°C), followed by *in situ* growth of δ-MnO_2. Increasing pyrolysis temperature transformed MnO_2 morphology into a 3D lamellar nanostructure, enhancing electrochemical properties. The MnO_2/LPC composite achieved 145 F g^{-1} at 1 A g^{-1} and retained a performance rate of 75.9%, demonstrating high capacitance and stability in symmetric supercapacitors (Lou *et al*. 2024). A ternary PPy/PANI/MnO_2 was synthesized by oxidative polymerization and optimized for supercapacitor electrodes. Structural and electrochemical characterizations confirmed high capacitance in 84% neutral electrolyte (309.61 F g^{-1} at 5 A g^{-1}) retention following 2500 cycles. A symmetric device achieved 181.5 F g^{-1}, 36.31 Wh kg^{-1} energy density, and low ESR (1.12 Ω), demonstrating excellent cyclic stability and power performance (Elumalai *et al*. 2024). A rGO–MnO_2 nanocomposite was prepared by hydrothermal synthesis, exhibiting uniform nanowire morphology and strong interfacial charge transfer. Electrochemical analysis showed high sensitivity toward histamine detection, while photocatalytic studies achieved 91.7% Eriochrome Black T degradation. The enhanced activity was attributed to efficient electron transfer from MnO_2 to rGO, supported by strong structural stability over multiple cycles (Susee *et al*. 2024).

Sm_3RuO_7 nanorods and Sm_3RuO_7–MnO_2 composites were synthesized by hydrothermal and blending methods. The XRD, XPS, and TEM confirmed phase purity and uniform dispersion. Electrochemical tests revealed superior capacitance for the composite (805 F g^{-1} at 5 mV/s, 802 F g^{-1} at 1 A g^{-1}) compared to pure Sm_3RuO_7 (326 F g^{-1}). The MnO_2 incorporation enhanced charge transfer and interfacial activity, resulting in excellent supercapacitive performance (Vidyalakshmi *et al*. 2024). Mo-doped MnO_2 cathode materials were synthesized hydrothermally using $KMnO_4$ to improve Zn–MnO_2 battery performance. Structural studies revealed α- and δ-MnO_2 phases with uniform Mo distribution. Doping (up to 5 mol%) enhanced specific capacity and rate capability in acidic electrolytes (pH 1.5), showing improved cyclic stability and discharge retention compared to undoped MnO_2 (Griščenko *et al*. 2024). Polyaniline and PANI/TiO_2 composites were fabricated using MnO_2 as an oxidizing agent to form nanofibrous structures by oxidative polymerization. Characterization confirmed porous morphology and strong interfacial bonding. Electrochemical studies revealed high capacitance (800.25 F/g for PANI and 1110 F/g for PANI/ TiO_2) with 95.3% retention after 1000 cycles, highlighting their potential in high-performance supercapacitors (Makhloufi *et al*. 2023). A carbon MnO_2/Fe_3O_4 nanocomposite was synthesized and characterized by FE-SEM, HRTEM, XRD, and FTIR. Electrochemical tests in 0.5 M Na_2SO_4 provide a high specific capacitance of 730 F/g at 4 A/g and excellent stability of only 17.7% loss after 5000 cycles. The symmetric device achieved 456 F/g, 160 Wh/kg energy density, and 400 W/kg power density, confirming efficient charge storage and conductivity (Sohouli *et al*. 2022).

Zn anodes of different particle morphologies were studied in NH_4Cl electrolyte to understand corrosion behavior in Zn/MnO_2 batteries. SEM and XRD revealed ZnO and $Zn(NH_3)_2Cl_2$ formation. Zn powder (>500 µm) paired with nanostructured MnO_2(NMD) cathode showed high stability (1.65 V, 109.72 mWh/g, <0.7% voltage drop), confirming morphology-controlled corrosion mitigation and improved battery performance (Moulaï *et al*. 2021). The α-MnO_2 nanorods were synthesized hydrothermally and evaluated in various electrolytes. The composite electrolyte (1 M Na_2SO_4 + 0.5 M KOH) yielded superior electrochemical performance with 570 F/g at 1 A/g and 80% capacitance retention after 10,000 cycles. The study demonstrated excellent ion diffusion, reversibility, and coulombic efficiency (~80%) suitable for durable supercapacitor applications (Jayachandran *et al*. 2021). Hybrid biocomposites incorporating fine granite and tamarind shell powders as reinforcements in epoxy resin were developed by compression moulding. Experimental compression tests revealed substantial improvement in mechanical strength with increasing filler content. The results suggest that these natural–mineral hybrid composites are effective for producing eco-friendly and mechanically robust materials (Girimurugan *et al*. 2022). Dimensional stable TiO_2–MWCNT composites with varying MnO_2 (5–15 wt%) were fabricated by powder processing and spark plasma sintering. Increasing MnO_2 improved electrochemical stability and anodic protection while lowering potential degradation. The SEM and XRD analyses confirmed dense, low-porosity anodic layers for 15 wt% MnO_2 composites, highlighting their suitability for corrosion-resistant electrodes (Lephuthing *et al*. 2021). ZIF-67-derived porous carbon hybridized with MnO_2 was developed and characterized for ORR catalysis. The CV, EIS, and chronoamperometry in 0.1 M KOH showed enhanced electrocatalytic activity and stability under oxygen-saturated conditions. The hybrid structure exhibited improved charge transfer and reduced impedance, suggesting strong potential as a cost-effective cathode material for alkaline fuel cells (Salahuddin *et al*. 2021).

Hydrothermally synthesized Fe_2O_3 nanorods exhibited a cubic crystalline structure with an average size of ~30 nm. Electrochemical analysis revealed high specific capacitance of 489 F/g on 10 mV/s and a low ESR value of 3.26 Ω, indicating efficient charge transport. The Fe_2O_3 electrodes demonstrated excellent stability, retaining high capacitance after 500 charge–discharge cycles, confirming their suitability for scalable and next-generation energy storage devices (Khawale *et al*. 2024). Nickel–cobalt ferrite ($NiCoFe_2O_4$) nanoparticles were incorporated into PVA/PVP matrices by solution casting to develop hybrid polymer nanocomposites for energy storage. Electrochemical analysis demonstrated a specific capacitance of 13.49 F/g at 1 A/g and 99.39% coulombic efficiency, highlighting $NiCoFe_2O_4$–PVA/PVP nanocomposites as promising candidates for flexible, renewable supercapacitor electrodes (Vadivel *et al*. 2022).

Despite the substantial research on transition-metal oxide-based electrode materials, most investigations rely on synthetic polymers or expensive carbonaceous supports, which impede large-scale, eco-friendly energy-storage development. Moreover, the synergistic interaction between biowaste-derived organic materials and MnO_2 nanostructures remains inadequately investigated, notably for their electrochemical and pseudocapacitive activity. In this regard, the present work offers a TSP–MnO_2 nanocomposite made using a simple and affordable co-precipitation technique, leveraging a biomass source as a natural carbon precursor. The novelty of the study lies in demonstrating enhanced specific capacitance, improved ionic conductivity, and reduced internal resistance compared to TSP, establishing this bio-derived MnO_2 hybrid as a sustainable and high-performance electrode material.

2. MATERIALS AND METHODOLOGY

2.1 Materials

Tamarind was collected from in and around Anthiyur, Tamil Nadu, India. Manganese dioxide with a purity of 99.9% and a molecular weight of 86.94 g/mol was synthesized in the laboratory by a regulated procedure. Deionized water, devoid of contaminants and with a C_{sp} not above 1 µS/cm was utilized throughout the study.

2.2 Methods

2.2.1 Synthesis of TSP and Manganese Dioxide

The collected seeds were thoroughly washed with deionized water to eliminate any adhering impurities and then they were dried in shade at room temperature for 1–3 days to eliminate residual moisture. After drying, the seeds were cooled to room temperature and eventually ground using a multifunctional grinder to obtain a fine powder (Shashank *et al*. 2021). The resulting powder was sieved through 125 µm mesh sieve to assure uniform particle size distribution. The prepared TSP was then stored in an airtight container and further employed for the green synthesis of TSP–MnO_2 nanoparticles (Fig. 1).

About 3.95 g of potassium permanganate ($KMnO_4$), 4.95 g of manganese chloride tetrahydrate ($MnCl_2{\cdot}4H_2O$), and 0.5 g of polyvinylpyrrolidone (PVP) were individually diluted with 75 mL of deionized water. The solution was entirely dissolved at ultrasonic dispersion, following which it was transferred into 100-mL stainless steel container lined with polytetrafluoroethylene. The process occurred in an oven in 100°C for duration of 6 hours. The liquid was allowed to cool naturally at ambient temperature for obtaining the black precipitate. The black precipitate was subsequently washed with distilled water. Following centrifugation at 8000 rpm for 10 minutes, the supernatant was removed to give MnO_2 powder, which was dried at 60°C for 10 hours (Abdullah *et al*. 2024).

2.2.2 X-ray Diffraction (XRD)

The XRD examination was conducted on both pure MnO_2 and TSP-MnO_2 nanocomposites utilizing the Bruker D8 Advance equipment. The measurements were recorded using an X-ray diffractometer with Cu Kα radiation, functioning at a current of 30 mA and voltage of 40 kV. The diffraction data were acquired within a 2θ range of 10° to 80° (Selvaraju *et al*. 2022).

2.2.3 Scanning Electron Microscope (SEM)

The morphological characterization of TSP-MnO_2 was performed using scanning electron microscopy (SEM) (Gemini-ZEISS, Germany) with an energy dispersive X-ray spectrometer (EDAX) (Geethalaxmi *et al*. 2024).

2.2.4 FTIR Analysis

The FTIR analysis was performed using an IRSpirit spectrometer (Shimadzu Corporation, Kyoto, Japan) over the 4000–400 cm^{-1} range at a resolution of 16 cm^{-1} (Jayasree *et al*. 2021).

2.2.5 Electrochemistry-cyclic Voltammetry (CV)

The electrochemical analysis of the produced TSP-MnO_2 nanocomposite electrode was conducted using CV to assess its capacitive and redox capabilities (Selvaraj *et al*. 2022).

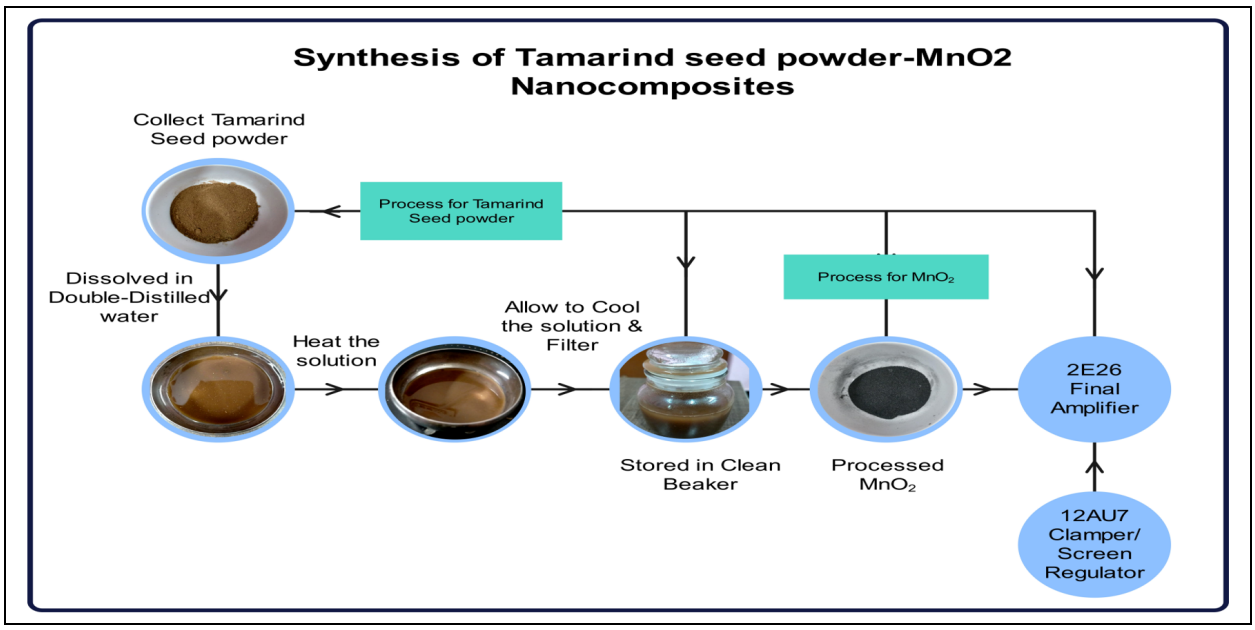


Fig. 1: Synthesis of TSP with MnO_2 nanocomposite materials

2.2.6 Galvanostatic Charge Discharge (GCD)

The charge-discharge properties of the TSP–MnO_2 nanocomposite electrode was assessed by GCD tests to ascertain specific capacitance and electrochemical stability (Sumedha *et al*. 2021).

2.2.7 Electrochemical Impedance Spectroscopy (EIS)

The interfacial charge transfer resistance and ion diffusion properties of the TSP–MnO_2 nanocomposite electrode were further examined using EIS.

3. RESULTS AND DISCUSSION

3.1 XRD Analysis

Fig. 2 illustrates the XRD of TSP-MnO_2 nanoparticles, which displayed only a broad peak around 2θ=20-25° suggesting the structure to be amorphous. The absence of sharp crystalline peaks indicates that the lignocellulosic components lack long range order. The crystalline structure of MnO_2 nanoparticles was studied by XRD. The prominent diffraction peaks were detected in MnO_2 at 2θ of 12.72°, 18.49°, 25.35°, 29.16°, 37.89°, 42.27°, 49.78°, 60.09, 65.12°and 69.48°, which can be well-indexed into (110), (200), (310), (211), (301), (411), (521), (541), and (222) facets, respectively. It is in good accord with XRD standard card JSPDF 44-0141 demonstrating tetragonal crystals of α-MnO_2. Moreover, no apparent peak relating to impurities was observed, showing high-purity of α-MnO_2

3.2 SEM Examination

The surface morphologies of fabricated samples was meticulously analyzed. The combination of TSP-MnO_2 nanocomposites facilitated a comprehensive study of particle size and structural features. The consistent shape of TSP-MnO_2 nanoparticles are illustrated in Fig. 3a, and 3b, by FESEM micrograph, revealing diminutive rods distributed randomly. This demonstrates the efficient decoration of TSP-MnO_2 nanorods, which, upon detailed observation, resemble the shape of seed. The TSP facilitates varied morphologies and sizes. This synthesis is distinguished by its flake-like sheet and consistent particle dispersion, which minimizes agglomeration formation. Dispersion optimization and particle morphology are crucial for applications. Distinct forms and shapes exhibiting increased surface area and porosity were identified in the TSP-MnO_2 nanocomposite material.

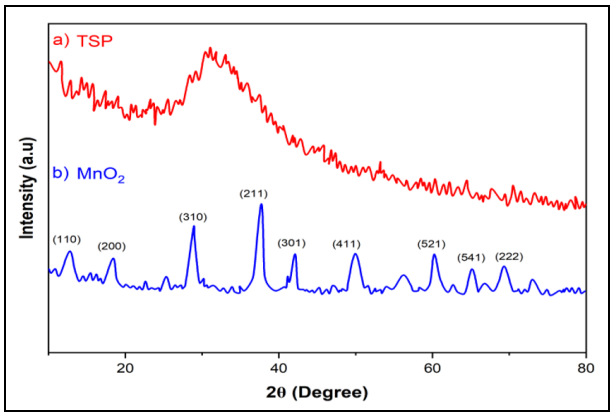


Fig. 2: XRD spectrum of TSP-MnO_2 nanocomposite

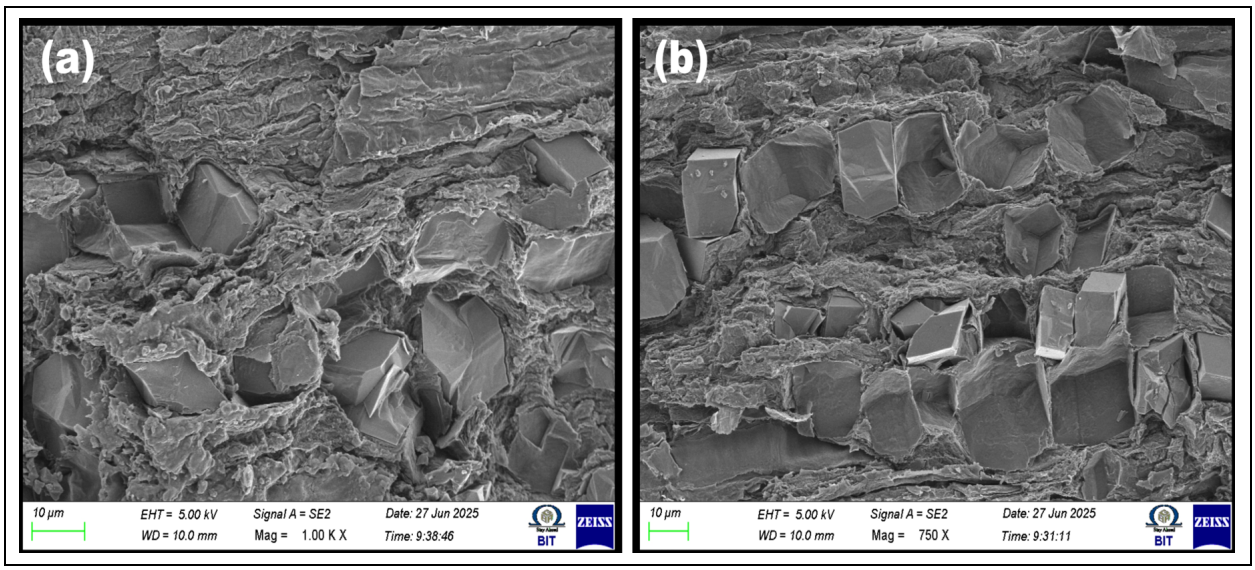


Fig. 3: FESEM image of synthesized TSP-MnO_2 nanocomposite

3.3 EDAX Analysis

The elemental analysis of the TSP-MnO_2 nanocomposite, conducted by EDAX, is illustrated in Fig. 4. Manganese dioxide comprises 0.74% atomic and 0.43 wt% of manganese; oxygen constitutes 48.92% atomic and 32.88 wt%; carbon accounts for 30.85% atomic percent and 15.21 wt%. The form, elemental composition, and structure of the specimens, together with the chemical structure of TSP-MnO_2 nanocomposite were examined to assess its potential effects in many applications, including its elemental decomposition. This comprehensive analysis improves the understanding of material's intrinsic composition and lays the groundwork for tailored applications at several technological and scientific domains.

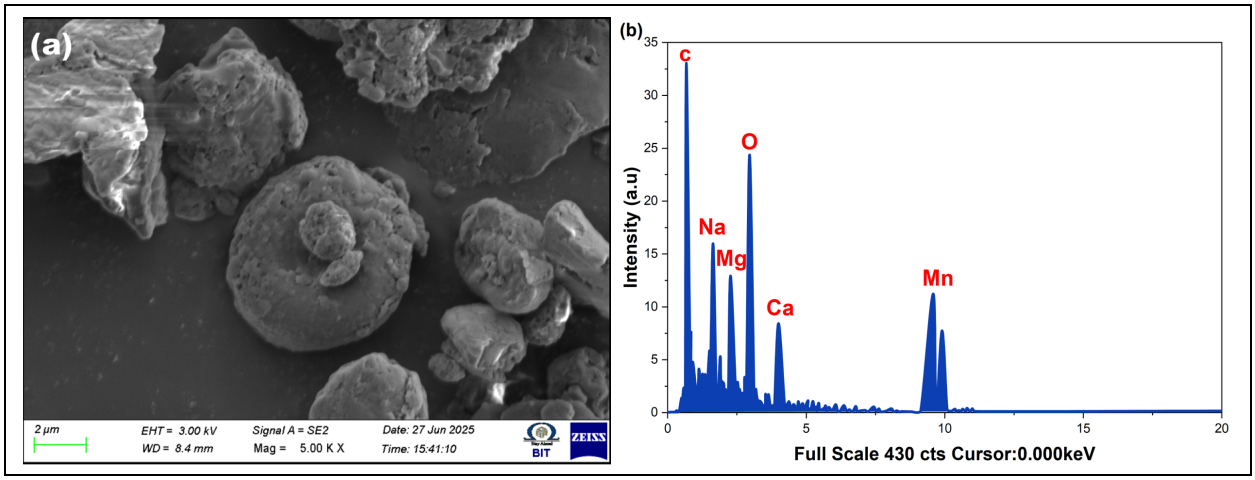


Fig. 4: Elemental composition analysis of TSP-MnO_2 nanocomposite

3.4 FTIR Examination

The TSP and its nanocomposite were studied using FTIR to detect surface functional group (Fig. 5, Table 1). The wide absorption band of 3367 cm^{-1} confirms the existence of -OH functional group. The structure of tamarind seed comprises polysaccharide polymers comprising galactose, xylose then glucose. The structures were accountable for the occurrence of -OH functional group in the spectrum of TSP. The peak at 1653 cm^{-1} and 1838 cm^{-1} are due to C-O and C=O stretching vibrations, respectively. A strong peak at 2975 cm^{-1} is due to C-H stretching. Specifically, peaks found in region of 700–800 cm^{-1} were suggestive of MnO_2 stretching vibration. The peaks at 3212 and 3486 cm^{-1} show the presence of hydroxyl groups, attributable to phytochemicals or other phenolic compounds. The peak at 1658 cm^{-1} was linked to C=N stretching vibration, revealing imine groups likely produced by amino acids. The peaks at 1426 and 1375 cm^{-1} reflect O–H bending vibrations, indicating the participation of hydroxyl group. The peak at 1040 cm^{-1} was attributed to C–O

stretching vibration. The peaks at 733 then 487 cm^{-1} are linked with alkene. These vibrational peaks confirm the inclusion of many phytochemicals and biomolecules. This spectral study shows the multifunctionality and complexity of components with TSP extract that lead to the stability and formation of MnO_2 nanoparticles. The MnO_2 stretching vibrations were seen around 606 and 765 cm^{-1}.

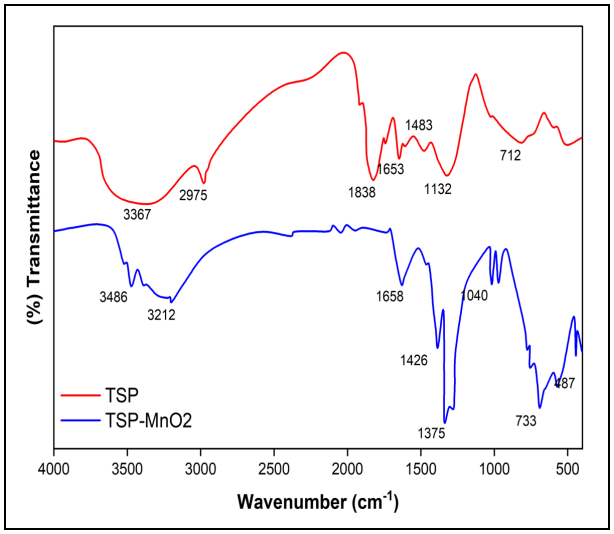


Fig. 5: FTIR spectra of TSP-MnO_2 composite and pure TSP

Table 1. FTIR spectra analysis of TSP /MnO_2 NPs

No	Functional Group	Vibrational Appearance	Absorption (cm^{-1})	Frequency Range
1	Alcohol	O-H stretching	Strong, broad	3486
2	Alcohol	O-H stretching	Strong, broad	3212
3	Imine/oxime	C=N stretching	Medium	1658
4	Carboxylic acid	O-H bending	Medium	1426
5	Phenol	O-H bending	Medium	1375
6	Primary alcohol	C-O stretching	Strong	1040
7	Alkene	C=C bending	Medium	733
8	Alkene	C=C bending	Strong	487
9	Metal oxide NPs	MnO_2	Sharp	606-765

3.5 Electrochemistry-cyclic Voltammetry (CV) Analysis

The TSP-MnO_2 nanocomposite electrode was fabricated by a systematic procedure aimed at enhancing stability and conductivity. The procedure commences with the application of a precisely prepared nanocomposite mixture combined with a poly(tetrafluoroethylene) (PTFE) binder onto a 1 × 1 cm conductive graphite sheet. The incorporation of PTFE improves the mechanical stability of the electrode, guaranteeing endurance at operational conditions. Activated carbon was integrated into the mixture to improve the electrical conductivity of the electrode. The use of N-methyl 2-pyrrolidone solvent were crucial, because it improves the uniform dispersion of components and increases overall conductivity of finished slurry. After preparing the slurry, it was applied to graphite sheet and dried. A three-electrode setup was constructed for electrochemical analysis, utilizing a 3 M KOH solution electrolyte. The CV curve for pure TSP demonstrates pseudocapacitive characteristics at different scan speeds, from 15 to 150 mV/s. This has quasi-rectangular form, signifying excellent charge storage characteristics over an extensive potential range, while some deviation is noticeable at elevated scan resolution (Fig. 6a). The CV curve for TSP-MnO_2 nanocomposite demonstrates pseudocapacitive activity (Fig. 6b). In contrast to pure TSP, the wider CV curve signifies enhanced capacitive performance and charge storage attributable to the inclusion of MnO_2 NPs. A bar graph illustrating the energy density (E_g) and specific capacitance (C_{sp}) of pure TSP at various scan rates is given in Fig. 6c.

The C_{sp} diminishes with an increase in scan rate, declining from 283.26 F/g at 10 mV/s to 215.26 F/g at 100 mV/s. Energy density also diminishes. Trends indicate diminished charge storing capacity at elevated scan speeds. A graph illustrating E_g and C_{sp} of the TSP-MnO_2 nanocomposite is shown in Fig. 6d. The maximum C_{sp} of 515.26 F/g on 10 mV/s demonstrates substantial enhancement compared to pure TSP, with values remaining notably elevated higher scan rates (315.95 F/g on 100 mV/s). Energy exhibits comparable trend, diminishing from 315.95 Wh/kg at 10 mV/s to 282.26 Wh/kg at 100 mV/s, underscoring superior execution of nanocomposite. The integration of MnO_2 nanoparticles into TSP increases the specific capacitance from 315.96 to 515.26 F/g and the energy density from 210.50 to 282.26 Wh/kg, attributed to an expanded surface area and enhanced conductivity. This leads to improved electrochemical performance, enabling rapid energy discharge and effective charge storage. In a previous study, a MnO_2–CuO–BaO (MCB) nanocomposite was synthesized hydrothermally at 80°C. Cyclic voltammetry in 1 M KOH exhibited pseudocapacitive behavior with 198 F/g capacitance at 10 mV/s, demonstrating the MCB composite as a potential electrode material for next-generation supercapacitors (Padmadevi *et al.* 2021).

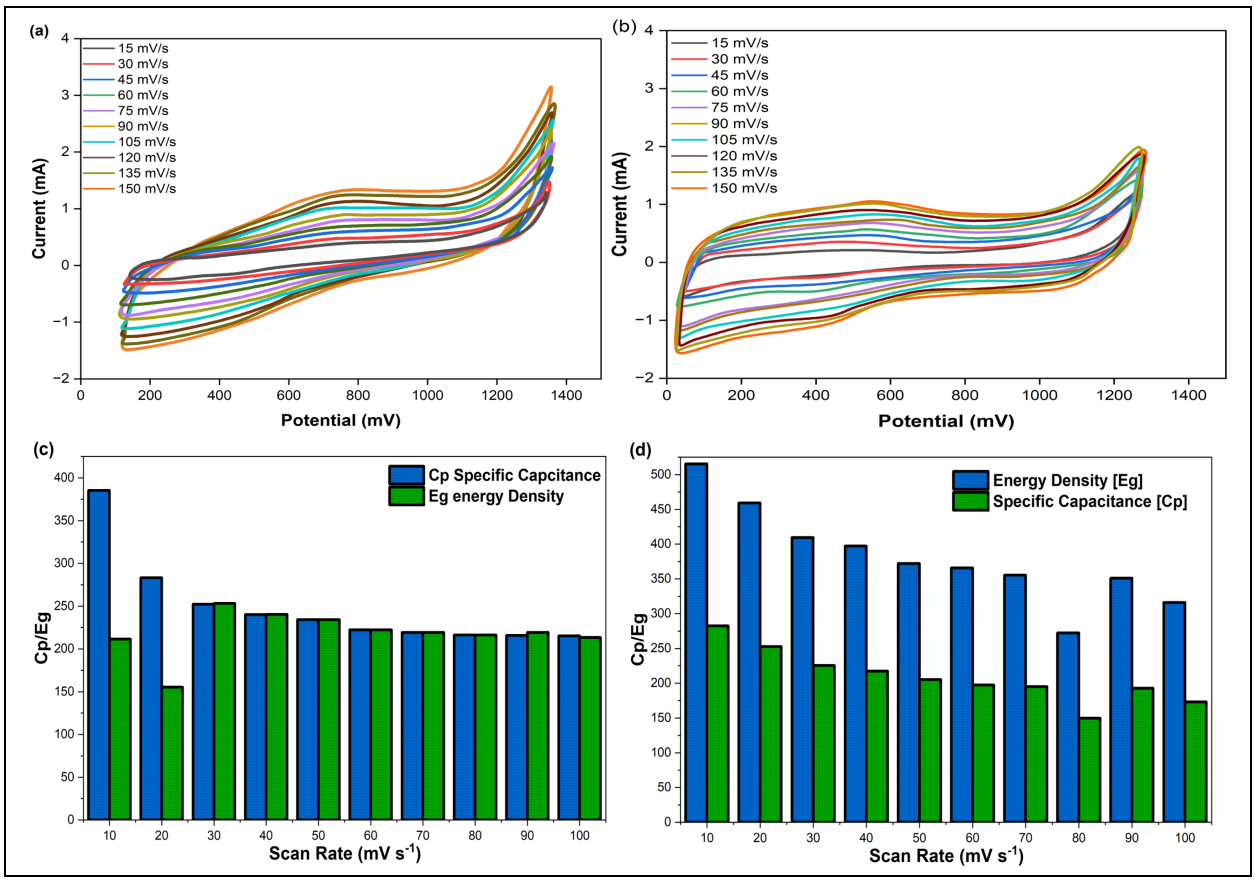


Fig. 6: Specific capacitance (Csp) and energy density (Eg) are shown in the CV diagram (a, b) and as a function of the scan rate (mV s.−1) (c, d)

3.6 Galvanostatic Charge Discharge

As illustrated in Fig. 7a and b, this study investigated galvanostatic charge–discharge curves of pure TSP (PT) and TSP-MnO_2 composite (TM) at current densities ranging from 2 - 20 A/g. Pure TSP has a discharge duration of 27 seconds at a density of 4 A/g, whereas TSP-MnO_2 has a release time of 17 seconds. This implies that pure TSP is more effective at maintaining charge at reduced current densities. The discharge durations for PT and TM diminish significantly as current density increases to 4 A/g, with PT lasting 3 seconds and TM lasting 6.5 seconds. This pattern remains consistent at 6 A/g, with TM exhibiting a 7-second duration and PT exhibiting a 2-second duration. Additionally, discharge durations for both materials experience a substantial decrease at current densities of 8 to 20 A/g with TM reducing to less than 1 second and PT decreasing to 2 seconds. Multiple scientific explanations contribute to the rapid reduction in discharge times. At elevated current densities, ion diffusion constraints are initially apparent. Particularly, at elevated current densities, electrode polarization effects are substantial. As a result of charge accumulation at the electrode surface, resistance within the electrode increases, which impedes ionic flow and results in shorter discharge durations. The structural integrity and conductivity of the material determine the polarization effect. Additionally, electrochemical efficacy is significantly influenced by mass transport constraints. The rapid extraction of ions and insertion surpass their transport to active sites at high current densities, particularly in materials with complex structures. A reduction in discharge duration is the result of the variation in ion transport rates. Fig. 7c and 7d illustrate the correlation among current density and specific capacitance, which shows that PT fluctuates between 7.2 and 1.0 F/g, while TM fluctuates between 9.1 and 5.1 F/g. The current density raises from 2 - 20 A/g. In a prior work, electrochemical studies showed superior capacitance for Polyaniline (PANI) –5%CdO (866 F/g by CV; 906.8 F/g by GCD) and low ESR, indicating efficient ion diffusion and high energy density (9.04 Wh/kg), making it a strong electrode material for supercapacitors (Anwar *et al.* 2022). Factors such as geometry, surface area, and material composition can account for the discrepancies in specific capacitance. The increase in initial capacitance values observed is due to the fact that the inclusion of MnO_2 in charge storage capacity and TM enhances ionic conductivity in comparison to PT. These discrepancies in performance among TM and PT underline the significance of modifying compositional and structural characteristics to comply with the energy demands.

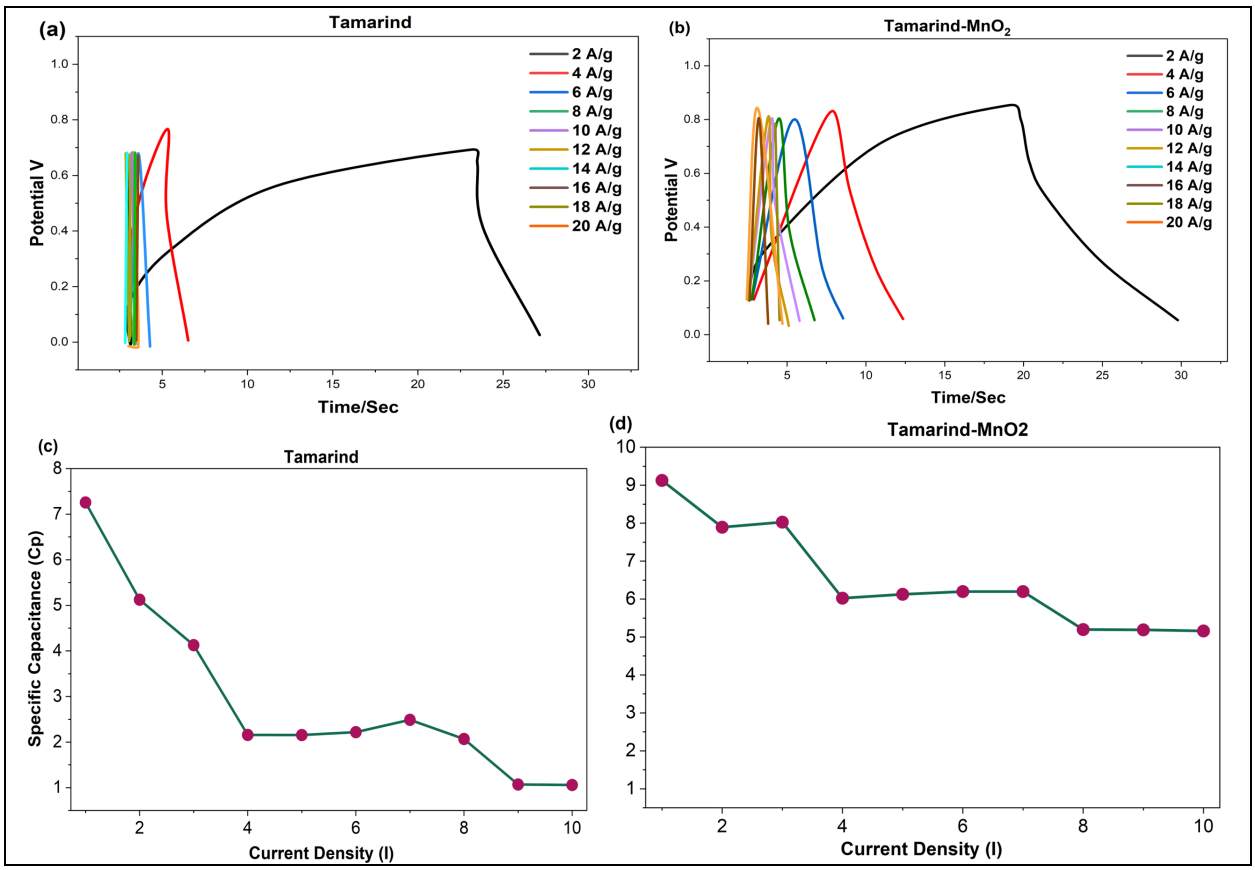


Fig. 7: GCD diagram of specific capacitance /current density for pure TSP and TSP-MnO_2 nanocomposites

3.7 Electrochemical Impedance Spectroscopy (EIS)

An effective method for examining electrical characteristics of materials and interfaces with a variety of environment is electrochemical impedance spectroscopy (EIS). It serves wide range of applications as biological sensing, fuel cell research and corrosion study. This study investigates the utilization of electrochemical impedance spectroscopy (EIS) to analyze pure TSP and TSP-MnO_2. AC impedance spectroscopy measured the electrical conductivity of the TSP-MnO_2 composite.

Fig. 8a and 8b depict the Nyquist plots of PT and TM at ambient temperature. Nyquist plots typically consist of two sections: a high-frequency portion and a low-frequency zone. Organic molecules can engage in redox processes, which involve the oxidation or reduction of the molecules. These reactions frequently occur at the electrode interface, resulting in a measurable current flow. An analogous circuit model can interpret the impedance study of the composite. The ionic conductivity of the electrolyte is indicative of resistance of the pure TSP system. According to the charge transfer resistance, the electron transfer efficiency at the interface of TSP and electrolyte is moderate, indicating moderate electrochemical reaction rates. Indicating the system's ability to accumulate charge at the interface, the double-layer capacitance is essential for energy storage applications. The Warburg impedance is a measure of the ion diffusion characteristics that significantly affect all reaction kinetics, particularly in electrochemical devices. Similar circuit characteristics for R_s, C_{dl} and W_0 are observed in comparison to the MnO_2 composite integrated with TSP. The charge transfer resistance is the predominant difference, as it lower than of pure TSP. The TSP-MnO_2 composite's reduced R_{ct} suggests that electron transmission has been substantially enhanced, thereby enhancing electrochemical activity and enabling expedited charge/discharge rates. These characteristics are most suitable for practical energy storage applications. Formula (1) was employed to determine the electrical conductivity (Shojaeifar *et al.* 2022).

$$\sigma = \frac{l}{R_b A} \mathrm{Scm^{-1}} \qquad \ldots (1),$$

where l is the material thickness, R_b is the bulk resistance and A is the electrode area. Pure TSP has an ionic conductivity of 3.4×10^{-4} S/cm, while the combined ionic conductivity of TSP and MnO_2 is shown in Fig. 8a and b. Pure TSP shows negligible conductivity; however, supplementation with MnO_2 notably improves ionic conductivity. This improvement is attributed to the impact of MnO_2, as evidenced by an increase in charge carriers.

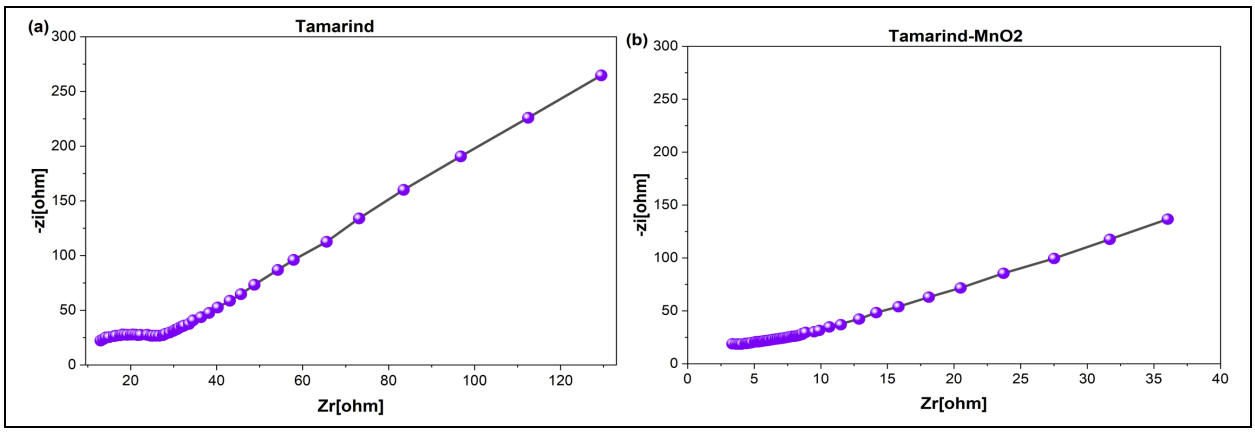


Fig. 8: Nyquist plot for (a) TSP and (b) TSP-MnO_2 nanocomposite

4. CONCLUSION

The successful synthesis of a TSP–MnO_2 nanocomposite through a simple co-precipitation method demonstrates its strong potential for energy storage applications. Structural and spectroscopic analyses confirm the formation of a crystalline MnO_2 matrix with effective incorporation of TSP-derived organic components, while microscopic observations reveal a heterogeneous morphology. Electrochemical studies indicate pronounced pseudocapacitive behavior, reflected in enhanced energy storage performance compared to pure TSP. The TSP–MnO_2 nanocomposite can be a promising electrode material for advanced supercapacitors, bridging the gap between batteries and conventional capacitors. Further improvements may be achieved through synthesis optimization and incorporation of conductive nanomaterials.

FUNDING

This research received no specific grant from any funding agency in the public, commercial, or not-for-profit sectors.

CONFLICTS OF INTEREST

The authors declare that there is no conflict of interest.

COPYRIGHT

This article is an open-access article distributed under the terms and conditions of the Creative Commons Attribution (CC BY) license (http://creativecommons.org/licenses/by/4.0/).

REFERENCES

Abdullah, M., John, P., Jabbour, K., Ahmad, M. I., Khan, S., Waheed, M. S., Albaqami, M. D., Sheikh, M., Ehsan, M. F. and Naeem, A. M. N., Improvement in capacitive performance of ZnS with MnO_2 via composite (ZnS/MnO_2) strategy developed by hydrothermal technique, *J. Energy Storage,* 78, 110034 (2024). https://doi.org/10.1016/j.est.2023.110034

Adarshgowda, N., Bhojya Naik, H. S., Vishnu, G. and Hareeshanaik, S., Green synthesized manganese-doped cobalt ferrite photocatalysts for light driven degradation of dye and optoelectronic studies, *Ceram. Int*., 50(12), 22060–22076 (2024). https://doi.org/10.1016/j.ceramint.2024.03.320

Anwar, N., Shakoor, A., Ali, G., Ahmad, H., Niaz, N. A., and Mahmood, A., Synthesis and electrochemical characterization of polyaniline doped cadmium oxide (PANI–CdO) nanocomposites for supercapacitor applications, *J. Energy Storage*, 55, 105446 (2022). https://doi.org/10.1016/j.est.2022.105446

Elumalai, P., Charles, J. and Kennedy, L. J., Fabrication of PPy/PANI/MnO_2-based electrode and its electrochemical evaluation for supercapacitor applications, *Ionics*, 30(11), 7397–7420 (2024). https://doi.org/10.1007/s11581-024-05794-w

Geethalaxmi, M., Kumar, U., Verma, V., Sunil, C. K., Rawson, A. and Venkatachalapathy, N., Effect of roasting on physicochemical, functional, thermal, pasting, and structural properties of TSP, *Food Chem. Adv*., 5, 100834 (2024). https://doi.org/10.1016/j.focha.2024.100834

Girimurugan, R., Loganathan, G. B., Sivaraman, G., Shilaja, C. and Selvaraju, M., Compressive behavior of tamarind shell powder and fine granite particles reinforced epoxy matrix-based hybrid bio-composites, *ECS Trans.*, 107(1), 7111–7118 (2022). https://doi.org/10.1149/10701.7111ecst

Griščenko, Ņ., Durena, R., Iesalnieks, M., Bērtiņš, M., Viksna, A. and Zukuls, A., Improvement of manganese dioxide cathode by molybdenum doping in highly acidic electrolyte, *J. Energy Storage*, 76, 109847 (2024). https://doi.org/10.1016/j.est.2023.109847

Jayachandran, M., Rose, A., Maiyalagan, T., Poongodi, N. and Vijayakumar, T., Effect of various aqueous electrolytes on the electrochemical performance of α-MnO_2 nanorods as electrode materials for supercapacitor application, *Electrochim. Acta*, 366, 137412 (2021). https://doi.org/10.1016/j.electacta.2020.137412

Jayasree, R., Senthil Kumar, P. S., Saravanan, A., Hemavathy, R. V., Yaashikaa, P. R., Arthi, P., Shreshta, J., Jeevanantham, S., Karishma, S., Valan Arasu, M. V., Al-Dhabi, N. A. and Choi, K. C., Sequestration of toxic Pb(II) ions using ultrasonic modified agro waste: Adsorption mechanism and modelling study, *Chemosphere*, 285, 131502 (2021). https://doi.org/10.1016/j.chemosphere.2021.131502

Khawale, V. R., Mayank, N., Ranade, R., Satishkumar, P., Haldar, B., Deepa, B., Saminathan, R., Veeramanikandan, P., Packirisamy, A. S. B. and Selvaraju, M., Study on electrochemical stability and charge transfer efficiency for the development of high-performance supercapacitors using iron oxide (Fe_2O_3) nanorods, *J. New Mater. Electrochem. Syst.*, 27(3), 163–171 (2024). https://doi.org/10.14447/jnmes.v27i3.a01

Lephuthing, S. S., Okoro, A. M., Ige, O. O. and Olunambi, P. A., Microstructural and electrochemical studies of spark plasma sintered multiwall carbon nanotubes reinforced TiO_2–MnO_2 based composite, *J. Mater. Res. Technol.*, 12, 894–903 (2021). https://doi.org/10.1016/j.jmrt.2021.03.003

Lou, R., Niu, T., Cao, Q., Zhang, Y., Lei, W., Lu, C. and Wang, Z., Preparation and electrochemical performances of in-situ growth of δ-MnO_2 on hierarchical porous carbon derived from LNP, *CIESC J.*, 43(2), 1013–1021 (2024). https://doi.org/10.16085/j.issn.1000-6613.2023-0295

Makhloufi, M. C., Benhaddad, L., Djelali, N. E., Metref, F., Amrane, C. and Hamidouche, F., Nanofibrous PANI/TiO_2 composite synthesized with sea urchin-shaped MnO_2 nanostructure for high-performance pseudocapacitors, *Russ. J. Electrochem.*, 93(9), 2360–2370 (2023). https://doi.org/10.1134/S1070363223090177

Moulaï, F., Hadjersi, T. and Achour, A., The effect of zinc shape on its corrosion mitigation as an anode in aqueous Zn/MnO_2 battery, *J. Electroanal. Chem.*, 886, 115140 (2021). https://doi.org/10.1016/j.jelechem.2021.115140

Padmadevi, B., Arivalagan, A., Khalifa, A. S., Shanmuganathan, R. and Kalaivani, T., Novel MnO_2–CuO–BaO metal oxide nanocomposite for high performance supercapacitors, *Process Biochem.*, 110, 176–180 (2021). https://doi.org/10.1016/j.procbio.2021.08.017

Purnama, S. K., Doewes, R. I., Elumalai, G., Azmi, S. H., Nuryadin, I. and Manshuralhudlori, Biosensor development in sports doping with dexamethasone, *Rev. Bras. Med. Esporte*, 29, e2022_0416 (2023). https://doi.org/10.1590/1517869220232901 2022_0416

Salahuddin, U., Iqbal, N., Noor, T., Hanif, S., Ejaz, H., Zaman, N. and Ahmed, S., ZIF-67 derived MnO_2 doped electrocatalyst for oxygen reduction reaction, *Catalysts*, 11(1), 1–14 (2021). https://doi.org/10.3390/catal11010092

Selvaraj, A. R., Raja, I. S., Chinnadurai, D., Rajendiran, R., Cho, I., Han, D. W. and Prabakar, K., Electrospun one-dimensional pseudocapacitive nanorods embedded carbon nanofiber as positrode and graphene wrapped carbon nanofiber as negatrode for enhanced electrochemical energy storage, *J. Energy Storage*, 46, 103731 (2022). https://doi.org/10.1016/j.est.2021.103731

Selvaraju, M., Rathinam, R., Saminathan, R., Deepalakshmi, R., Gopal, M., Justin Maria Hillary, J. J. M., Nanthakumar, S., Ganvir, V. Y.,and Singh, P., Analysis of spectroscopic, morphological characterization and interaction of dye molecules for the surface modification of TiB_2 nanoparticles, *J. Nanomater.*, 2022, 1033216 (2022). https://doi.org/10.1155/2022/1033216

Shahsank, M., Bhojya Naik, H. S., Sumedha, H. N. and Nagaraju, G., Implementing an in-situ carbon formation of MoO_3 nanoparticles for high performance lithium-ion battery, *Ceram. Int.*, 47(7), 10261–10267 (2021). https://doi.org/10.1016/j.ceramint.2020.07.241

Shashank, M., Bhojya Naik, H. S., Patil, S. B., Viswantha, R. and Nagaraju, G., Green synthesis of molybdenum oxide nanoparticles: Advanced electrode material for electrochemical lithium storage, *Microchem. J.*, 171, 106818 (2021). https://doi.org/10.1016/j.microc.2021.106818

Shojaeifar, M., Askari, M. B., Hashemi, S. R. S. and Di Bartolomeo, A., MnO_2–NiO–MWCNTs nanocomposite as a catalyst for methanol and ethanol electrooxidation, *J. Phys. D: Appl. Phys.*, 55(35), 355301 (2022). https://doi.org/10.1088/1361-6463/ac7619

Sohouli, E., Adib, K., Maddah, B. and Najafi, M., Preparation of a supercapacitor electrode based on carbon nano-onions/manganese dioxide/iron oxide nanocomposite, *J. Energy Storage*, 52, 104987 (2022). https://doi.org/10.1016/j.est.2022.104987

Sumedha, H. N., Alsaiari, M. A., Jalalah, M. S., Shashank, M., Alharthi, F. A., Ahmad, N., Algethami, J. S., Vishwanth, V. and Nagaraju, G., Rapid microwave synthesis of β-$SnWO_4$ nanoparticles: An efficient anode material for lithium ion batteries, *Crystals*, 11(4), 334 (2021). https://doi.org/10.3390/cryst11040334

Susee, S. K., Sandhya, S., Senthil, K. M. and Rajan, B., Reduced graphene oxide–MnO_2 nanocomposites by hydrothermal method for histamine sensor and photocatalytic activity, *J. Mater. Sci.: Mater. Electron.*, 35(30), 13677 (2024). https://doi.org/10.1007/s10854-024-13677-z

Thiam, B. and Savadogo, O., Effects of silico-tungstic acid on the pseudocapacitive properties of manganese oxide for electrochemical capacitors applications, *Decarbon*, 6, 100066 (2024). https://doi.org/10.1016/j.decarb.2024.100066

Vadivel, V., Murugan, A., Shameem, A., Thangarasu, S. and Sultan, S. A., A facile microwave-assisted combustion synthesis of $NiCoFe_2O_4$ anchored polymer nanocomposites as an efficient electrode material for asymmetric supercapacitor application, *J. Energy Storage*, 48, 103965 (2022). https://doi.org/10.1016/j.est.2022.103965

Vidyalakshmi, Y., Vaishali, M. S. and Geetha, D., Synthesis and supercapacitor performance of Sm_3RuO_7 nanorods and Sm_3RuO_7/MnO_2 nanocomposite, *J. Mater. Sci.: Mater. Electron.*, 35(7), 12191 (2024). https://doi.org/10.1007/s10854-024-12191-6

Zabielaite, A., Kepenienė, V., Šimkūnaitė, D., Stagniūnaitė, R., Jasulaitienė, V., Stalnionis, G., Vaičiūnienė, J., Tamašauskaitė-Tamašiūnaitė, L. and Norkus, E., MnO_2 nanoparticles supported on graphitic carbon nitride as an electrocatalyst for oxygen reduction and evolution, *New J. Chem.*, 48(46), 19389–19402 (2024). https://doi.org/10.1039/d4nj03407d